Structured Polyethylene Nanocomposites: Effects of Crystal Orientation and Nanofiller Alignment on High Field Dielectric Properties

Bo Li [1], C. I. Camilli [1, †], P. I. Xidas [1,2], K. S. Triantafyllidis [2], E. Manias [1,*]

[1] Materials Science and Engineering, Penn State University, University Park, PA 16802, U.S.A
[2] Chemistry Department, Aristotle University of Thessaloniki, GR54006 Thessaloniki, GREECE
[*] address correspondence to manias@psu.edu; [†] undergraduate student.

ABSTRACT

In previous work we have shown that aligned high aspect-ratio (pseudo-2D) nanofillers can yield large dielectric breakdown strength (E_{BD}) improvements for a nanocomposite with a low-crystallinity polyethylene matrix. Here, we report a systematic study which delineates the contributions of the aligned inorganic fillers and of the aligned polymer crystallites in the overall E_{BD} improvement achieved in the nanocomposites. Specifically, extrusion blown-molded polyethylene/montmorillonite nanocomposite films were cold-stretched to various strains, to further align the nanoparticles parallel to the film surface; this filler alignment is accompanied by a commensurate alignment of the polymer crystallites, especially those heterogeneously nucleated by the fillers. A systematic series of films are studied, with increased extent of alignment of the fillers and of the crystalline lamellae (quantified through Hermans orientation order parameters from 2D X-ray diffraction studies) and the aligned structure is correlated to the electric field breakdown strength (quantified through Weibull failure studies). It is shown that aligned pseudo-2D inorganic nanofillers provide additional strong improvements in E_{BD}, improvements that are beyond, and added in excess of, any E_{BD} increases due to polymer-crystal orientation.

INTRODUCTION

Electrical breakdown strength (E_{BD}) is an important property for dielectric materials and insulators in various applications from mobile electronic devices, stationary power systems, to hybrid electric vehicles. Manufacturing of commercial dielectric films employs biaxial stretching to improve the dielectric breakdown strength (E_{BD}) of semicrystalline polyolefins, in particular for capacitor polypropylene and PVDF films. This methodology capitalizes on the strain-induced orientation of the crystallites in these films, and necessitates high purity and high crystallinity polymers, where E_{BD} is to be substantially improved. Although it has long been accepted that the breakdown mechanisms are generally associated with electronic avalanche, thermal runaway, electromechanical failure, and partial discharge [1, 2], in real systems more than one of these mechanisms can be, and usually are, coupled to determine the overall breakdown behavior. In addition, the inherently stochastic nature of the electrical breakdown makes the prediction and design of high-performance polymer dielectrics even much more complicated.

For polymer dielectrics, the crystallinity and crystal morphology have significant impacts on E_{BD}. Generally, compact and space-filling spherulites within a strong matrix phase are favorable for improving the electrical strength [3, 4]; lamellae oriented perpendicular to the insulation-electrode interface can contribute to further improve the insulation properties [5, e.g.], which most commonly originates from the higher resistance to electrical treeing across

crystalline lamellae (as, for example, can be revealed in TEM studies of electrical treeing initiation [6]). Along these lines, biaxial orientation of insulating crystalline polymer films is commonly employed to achieve high-E_{BD} (e.g. biaxial oriented polypropylene, BOPP). However, this approach necessitates high crystallinity and high purity polymers and, thus, removes from dielectric applications many low-crystallinity polymers with otherwise excellent engineering properties. At the same time, recent experiments and theoretical work have confirmed that the addition of pseudo-2D nanofillers in a non-random/prescribed morphology [7], can impart similar functionalities and enhancements, and for dielectrics oriented montmorillonite (MMT) nanoplatelets, for example, can improve the breakdown strength of polymer-matrix composites [8-10]. In previous work the controlled oriented arrangement of MMT fillers at the micro- and macro- scales, (oriented agglomerates and single layers) can yield substantially improved E_{BD} performance under high electric field [8-10], whereas the respective composites with randomly dispersed (non-oriented) fillers and everything else remaining the same showed little or no improvement in E_{BD} [10]. The higher E_{BD} strength was attributed to the more efficient obstruction of the mobile charge carrier motion by the oriented inorganic fillers (i.e., more tortuous pathways and more effective barriers for electrical treeing); given that together with the filler orientation these films also have an accompanying polymer crystallite orientation, there remains an open question on the relative importance of the oriented inorganic nanofillers vs. the oriented polymer crystallites [10].

Here, we report a systematic study which delineates the contributions of the aligned inorganic fillers and of the aligned polymer crystallites in the overall E_{BD} improvement, and we show that aligned pseudo-2D inorganic nanofillers provide additional strong improvements in E_{BD}, improvements that are beyond, and added in excess of, any E_{BD} increases due to polymer-crystal orientation.

EXPERIMENTAL DETAILS

The polyethylene (PE) here is a Dow Integral polyolefin [a nucleated (high-crystallinity) 80/20 blend of LLDPE/LDPE (linear low density PE/low density PE)]. The layered-silicate fillers were commercial (Nanomer grade, purchased from Nanocor) materials of organo-montmorillonites (o-MMT), with a nominal cation exchange capacity of 1.0 meq/g and were organically modified with dimethyl-dioctadecyl-ammonium surfactants. These organoclays were first dispersed at 25 wt% inorganic loading with a twin-screw extruder in maleic anhydride functionalized PE (a 0.26 wt% MAH-graft-LLDPE, $\bar{M}_w$=67000 g mol^{-1} and $\bar{M}_w/\bar{M}_n$=6.1). Nanocomposites were subsequently produced by letting down these PE-MAH/o-MMT concentrates by PE, at a final 6 wt% and 9 wt% o-MMT concentrations at commercial blown film line (Pliant Corp.); unfilled PE films were also processed under the same conditions.

Films were allowed to fully crystallize at room temperature for at least 4 weeks and were then cold-stretched along their machine direction by a tensile apparatus (Instron 5566); wide 5-10cm strips were uniaxially strained at room temperature and low strain rates (10 mm/min for the composite and 15 mm/min for the polymer) in order to achieve uniform deformation.

Wide-angle X-ray diffraction (WAXD) was carried out in a Rigaku D/MAX Rapid II instrument equipped with a 2D-detector and a graphite monochromator, using a 100μm pinhole collimator, a 127.4 mm sample-to-detector distance, and Cu K$\alpha_{1,2}$ radiation (λ=1.5418 Å). The films were measured both with the X-ray beam normal to the film surface (face-on XRD) and with the X-ray beam parallel to the film surface (edge-on XRD). A Leica Ultracut UCT

Microtome with cryoattachment was used for sectioning TEM specimens, which were imaged in a Jeol JEM-2010 TEM with LaB_6 emitter, operated at bright field at an accelerating voltage of 200 kV. Dielectric breakdown measurements were performed on a TREK P0621P instrument, after the film specimens were sandwiched between a one-side conducting polypropylene tape (top electrode) and a copper plate (bottom electrode); all specimens were tested under a dc voltage ramp of 500 V/s (more details can be found [11]).

RESULTS AND DISCUSSION

The dispersion and morphology of the o-MMT nano platelets in the PE matrix were evaluated by TEM. Figure 1(a) shows the bright field TEM of the composite films containing 6 wt% o-MMT, as produced in the industrial extrusion blow-molding line.
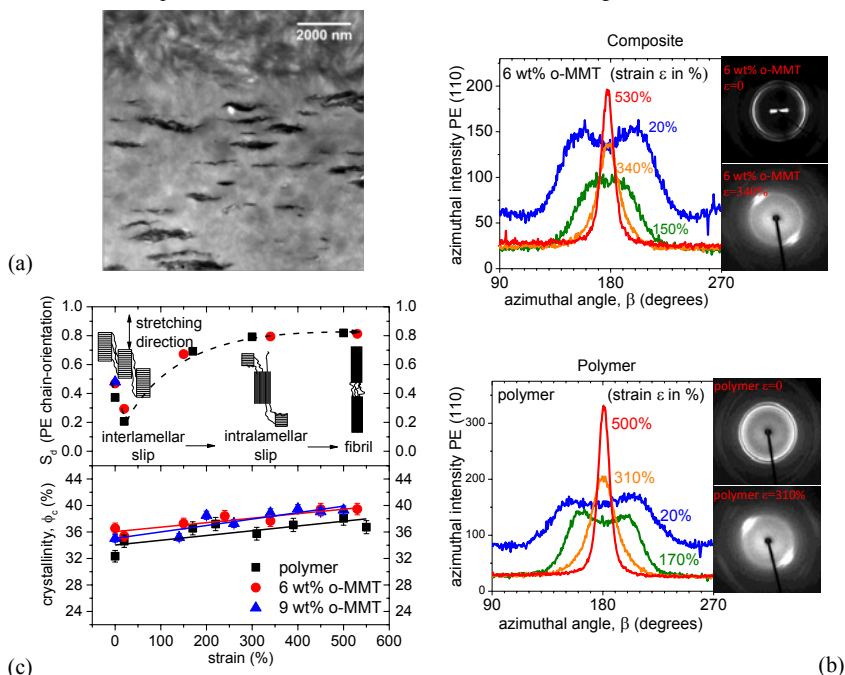

Figure 1. (a) TEM image of the 6 wt% nanocomposite film (without cold-stretching). (b) Azimuthally integrated intensities of the PE (110) diffraction peaks with increased strains (insets: 2D XRD patterns of the films, before and after cold stretching). (c) Order parameters of the 001 PE direction (polymer chain orientation) and polymer crystallinity *vs.* strain.

Large MMT agglomerates and smaller MMT tactoids (consisting of a few layers down to a single layer) are dispersed uniformly throughout the PE matrix, with a strong preferential alignment along the flow direction (filler platelets are parallel to the film surface). This filler orientation, defined by the shear rates of the film-blowing processing, is mostly retained after PE

relaxes and fully crystallizes, because the large μm-scale lateral dimension of MMT prevents marked MMT rearrangement. For the same reason, the filler orientation/structure is also retained after cold-stretching, i.e., there are no visible differences in the TEM images of the strained *vs.* non-strained films; hence, 2D XRD was employed to quantify the excess filler alignment/orientation (*vide infra*). The excess strain-induced crystallization is also limited (the crystallinity increases by less than 4% for each system over the entire strain range: 0-600% uniaxial strain, and the difference in crystallinity between the various systems is about 3% across all specimen films, as quantified by DSC); not surprisingly, as the polymer matrix is highly heterogeneously nucleated, which already maximizes the crystal fraction, even before the MMT addition and the uniaxial stretching.

Orientation (of either the filler or the polymer crystal) can be quantitatively assessed by the Hermans orientation function S_d of specific diffracted peaks from 2D-XRD patterns:

$$S_d = \frac{3<cos^2\phi>-1}{2} \quad \text{with} \quad <cos^2\phi> = \frac{\int_0^{\pi/2} I(\phi)cos^2\phi sin\phi d\phi}{\int_0^{\pi/2} I(\phi)sin\phi d\phi} \tag{1}$$

where I(ϕ) are radial intensities; the radial ϕ is the defined as: $cos(\phi) = cos(\beta)cos(\theta)$ with β being the azimuthal angle (I(β) is the experimental azimuthal intensity, Fig.1(b)) and θ being the usual Bragg angle (diffraction peak located at 2θ). The order parameter (S_d) can be calculated for any diffraction peak (*hkl*) given its background-corrected azimuthal intensity I(β), and S_d=0 denotes a randomly oriented *hkl* plane; S_d=−0.5 a plane oriented along the reference axis (symmetry axis); whereas S_d=1 a plane perfectly perpendicular to the reference axis. Figure 1 (b) shows the recorded 2D XRD patterns for the films before and after stretching (inset panels), along with the corresponding azimuthal diffraction-intensities for the 110 plane of PE. The azimuthal narrowing of the crystal diffraction bands in the 2D-XRD pattern serves as a clear indication of increased crystal orientation [12]. For the orthorhombic PE crystal structure here, the lamellae surfaces are perpendicular to the 001 chain orientation, which in absence of *00l* XRD reflections is calculated from the order parameters of the 200 and 110 diffracted peaks as usual [13]: $<cos^2\phi>_{00l} = 1 - 0.555 <cos^2\phi>_{200} - 1.445 <cos^2\phi>_{110}$

where the $<cos^2\phi>_{00l}$ is obtained from the measured $<cos^2\phi>_{200}$ and $<cos^2\phi>_{110}$. The order parameter (S_d) for the chain orientation 001 is plotted in Figure 1(c). As shown in Fig 1(c), the blown films (strain=0) already exhibit a certain degree of chain orientation, due to the film processing method; with increasing uniaxial strain there appears an initial drop in the 001 order parameter (reflecting a reduced alignment for crystalline chains) followed by a monotonic, albeit non-linear, strain-induced increase in orientation, along the draw direction. This is typical for PE, and has been reported before [14,15,e.g.], where at small strains (<20% strain), an affine deformation of spherulites takes place by interlamellar shearing [14, 15], and the tie chains are drawn along the stretching direction, rotating and shearing the rigid lamellae such that their large lateral surfaces are forced to gradually turn parallel to the stretching direction (depicted schematically in Fig 1(c), first stage interlamellar slip). Upon crossing the yield point, for larger strains (>20% strain), the deformation mechanism changes to an irreversible intralamellar-slip, towards the formation of fibrillar structures (Fig 1(c)). Interestingly, the organoclay nanofillers do not alter this chain orientation, as evidenced by the similar order parameters and trends for polymer *vs.* composite films, therefore, allowing the use of the strain value as a measure of crystal orientation for both unfilled PE films and composites.
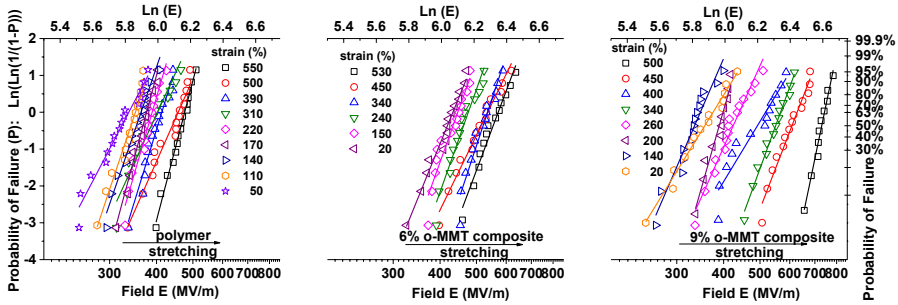
Figure 2. Weibull distribution of the experimentally observed breakdown strengths (E_{BD}) for the polymer and composites as a function of uniaxial strain (20-550% strain, marked in the legend).

The distribution of experimentally observed breakdown electric fields (E) can provide the characteristic dielectric breakdown strength E_{BD} of a system through the framework of Weibull statistics [16] (equation 2), from the raw data (Fig 2).

$$P(E_{BD}, \beta_w, E) = 1 - exp(-(\frac{E}{E_{BD}})^{\beta_w}) \tag{2}$$

where E_{BD} is the characteristic breakdown strength (defined as the electric field which corresponds to a cumulative failure probability P ~63.2%); and the Weibull modulus (β_w slope in Fig 2) is a measure of the scattering of the experimental data. The improvement in E_{BD} is obvious in both polymer and composite films (as a systematic shift of the raw data to higher fields), whereas the Weibull modulus (slope in Fig 2) remains comparable in all films and strains. The Weibull characteristics are summarized in Fig. 3.

From the E_{BD} data of the unfilled films (Fig. 3) we see that increasing the crystal orientation results in higher E_{BD} values, quantifying the effect of oriented polymer crystallites. This response and trend are in agreement with the typical behavior of oriented semicrystalline polymer films [5,6,10,17,18], and which is attributed to the barrier effects of the oriented/aligned crystallites, causing more tortuous pathways for the electrical treeing around them [5, 6].

The comparison of the unfilled films *vs.* the 6 wt% o-MMT nanocomposites, on the other hand, provides the effect of the oriented fillers; as shown in Fig 3. The addition of highly-oriented 2D nanofillers

Figure 3. Weibull breakdown strength (E_{BD}, top) and Weibull modulus (β_w, bottom) as a function of strain.

shifts the E_{BD}(strain) curve towards higher E-fields in a markedly parallel fashion (6 wt% nanofiller improves E_{BD} by *ca.*100 MV/m for all strains/alignments). This behavior denotes an additional amount of barrier (additional amount of electrical treeing path tortuosity) in a straight-
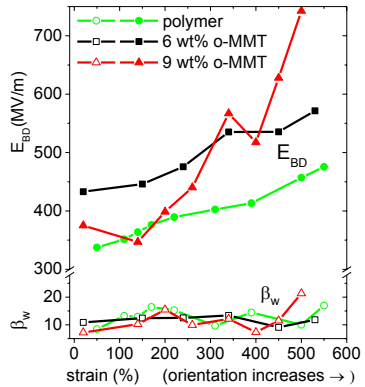
forward superposition/ synergistic manner to the oriented polymer crystal effect, a supposition which is also supported by the comparable β_W values for the two sets of films (Fig 3 bottom).

For the higher (9 wt%) filler concentration, the composite films start showing signatures of percolation (of fillers and polymer-crystallites), and the E_{BD}(strain) curve deviates from the shape of the unfilled PE and the low filler-loading composites; this deviation is becoming substantially pronounced at large strains ($\varepsilon>\sim260\%$) when the aligned fillers eventually establish a macroscopic barrier structure across the film, leading to a substantially increased E_{BD}.

CONCLUSIONS

Low crystallinity PE-MMT nanocomposites were oriented by cold-stretching to quantify the influence of (a) polymer-crystal orientation and of (b) pseudo-2D nanofillers alignment, on the electric field breakdown performance. As expected, crystal orientation improves E_{BD} in unfiller polymer films. Incorporation of oriented fillers provides an additional non-trivial increase in E_{BD} superimposed on the strain-induced E_{BD} improvements (fillers acted as additional independent barriers, synergistically adding to crystal orientation). At high filler concentrations and high strains/orientations, the onset of percolation was observed through a substantial E_{BD} improvement (suggesting the formation of macroscopic barriers).

ACKNOWLEDGMENTS

REFERENCES

1. J.C. Fothergill, *Electrical degradation and breakdown in polymers*. (IET, 1992).
2. A.R. Blythe, *Electrical properties of polymers*. (Cambridge University Press, 2005).
3. I.L. Hosier, A.S. Vaughan, S.G. Swingler, *J Polym Sci B: Polym Phys* **38**, 2309 (2000).
4. C.D. Green, Ph.D. thesis, University of Southampton, 2008.
5. T.Tanaka, T.Okamoto, N.Hozumi, K.Suzuki, *IEEE Trans Dielectr Electr Insul* **3**, 345 (1996)
6. N.Hozumi, M.Ishida, T.Okamoto, *et al.*, *IEEE Trans Dielectr Electr Insul* **25**, 707 (1990).
7. R.A. Vaia, J.F. Maguire, *Chemistry of Materials*, **19**, 2736 (2007).
8. J.K. Nelson, Y. Hu, *J Phys. D-Appl. Phys.* **38** (2), 213-222 (2005).
9. G. Polizos, V. Tomer, E. Manias, C.A. Randall, *J Appl. Phys.* **108**, 074117 (2010).
10. V. Tomer, G. Polizos, C.A. Randall, E. Manias, *J Appl. Phys.* **109**, 074113 (2011).
11. V. Tomer, C.A. Randall, *J Appl. Phys.* **104,** 074106 (2008).
12. J. Che, C. R. Locker, S. Lee, G. C. Rutledge, *et al.*, *Macromolecules*, **46** (13), 5279 (2013).
13. Z.W. Wilchinsky, *J Polym. Sci. Part B: Polym. Phys.* **6** (1), 281-288 (1968).
14. T. A. Huy, T. Luepke and H.-J. Radusch, *J Appl. Polym. Sci.* **80**, 148 (2001).
15. K. Sasaguri, S. Hoshino, R.S. Stein, *J Appl. Phys.* **35**, 47-54 (1964).
16. W. Weibull, *Journal of applied mechanics* **18**, 293-297 (1951).
17. K. Yahagi, *IEEE Trans Electr Insul*, **EI-15**, 241 (1980).
18. S. Sung-Ik, C. Dae-Hee, Y. Bok-Hee, T. Takahashi, T. Okamoto, Proceedings of 2005 International Symposium on *Electrical Insulating Materials* (ISEIM 2005).